Progress In Electromagnetics Research M, Vol. 119, 1–12, 2023

Design of a Metasurface Inspired Circularly Polarized Dual-Band Compact Antenna for Biomedical Applications

Umhara Rasool[1], Javaid A. Sheikh[1, *], Shazia Ashraf[1], and Gh. J. Qureshi[2]

Abstract—In this communication, a compact metasurface-based circularly polarized antenna with inverted L-shaped slots engraved in the ground is proposed for biomedical applications. The prospective antenna operates in the two frequency bands covering Medical Device Radio Service (Med Radio) and Industrial, Scientific, and Medicine (ISM) bands with center frequencies of 2.45 GHz and 4.1 GHz, respectively. The impedance bandwidth of 14.4% and 42.5%, peak gain of 3.04 dB, and axial ratio (AR) bandwidth of 0.3 GHz and 1.1 GHz in the two frequency bands (2.31–2.67 GHz and 3.28–5.04 GHz) are obtained respectively on mounting antenna on a human body. For validating the prospective design, an antenna with the size of $0.264\lambda_0 \times 0.264\lambda_0 \times 0.014\lambda_0$ was fabricated on a Rogers RT/Duroid 6002 substrate, and measurements were done in different scenarios. Link budget analysis of the device was also done for ensuring its communication ability.

1. INTRODUCTION

Biomedical engineering has contributed enormously to the welfare of human society wherein improvement in diagnosis, treatment, and prevention techniques of human diseases has been extensively worked upon in the last few decades. In particular, the wide usage of wirelessly connected devices (implantable or on-body) meant for bio-sensing, drug infusion, telemetry, stimulation, organ control [1], and bionic applications has revolutionized this sector, and thereof there is a need for comprehensive research in this area. The performance of the system designed for any particular biomedical application is determined by the efficacy of its principal component. The principal component in the biomedical system is the antenna which is assigned the task of bidirectional data transfer with the external control equipment. It is observed that the electromagnetic response of the biomedical antenna gets heavily impacted in the presence of the human body due to its lossy and dispersive nature. Furthermore, it needs to be noted that due to human body movements, there is a degraded performance in linearly polarized antennas due to polarization mismatch leading to inefficient data transfer. A common acceptable design for different patients for a particular application is a daunting task due to the difference in the anatomy of patients [2, 3]. So, it can be concluded that the antenna designed for any biomedical application needs to satisfy some basic design criteria which include compactness, bio-compatibility, safety of the patient in terms of Specific Absorption Rate (SAR), sufficient radiation efficiency, resistance to detuning effect, efficient powering of antenna, and circular polarization [4].

With incorporation of metamaterial structures in the design of antennas, the compact size, high gain, and multiband operation could be achieved simultaneously with minimum trade-offs. In [1], authors utilized metamaterial loaded superstrate for achieving high gain and wide 3 dB Axial Ratio (AR) bandwidth. Authors in [19, 20, 23] have achieved miniaturised size of the antenna by utilizing the concept of zeroth order resonance and wide fractional bandwidth at zeroth-order resonance (ZOR)

Received 1 June 2023, Accepted 17 August 2023, Scheduled 6 September 2023

* Corresponding author: Javaid Ahmad Sheikh (sheikhjavaid@uok.edu.in).

[1] Post Graduate Department of Electronics and Instrumentation Technology, University of Kashmir, India. [2] Department of Higher Education, Government of Jammu and Kashmir, India.

frequency. A Closed Ring Resonator loaded 4×1 metamaterial (MTM) array antenna with coplanar waveguide (CPW) feeding is proposed in [21]. The reported antenna offers a peak gain of 5.10 dBi, fractional bandwidth of 10.18%, and compact footprint area of $0.41\lambda_0 \times 0.69\lambda_0$. An electric field driven logic circuit (LC) resonator ground plane is utilized in [22] for achieving compact size, high directivity, and gain.

For biomedical applications, a CPW-fed circularly polarized (CP) wearable antenna backed by an artificial magnetic conductor (AMC) array is proposed in [5]. In this work, the authors have utilized an additional layer of AMC for achieving high gain and low SAR. In another communication, authors have reported a high gain, dual-band, and miniaturized CP implantable antenna for biomedical applications. The Planar Inverted-F-Antenna (PIFA) is integrated with an MTM-loaded superstrate for improving the gain and axial ratio of the designed PIFA. In [6], authors have proposed a circularly polarized implantable antenna for biotelemetry applications working in the Industrial, Scientific, and Medicine (ISM) band. The radiating patch of the prospective design in [6] is circular in shape with slots embedded in the ground for achieving Circular Polarization. The antenna operates either in right hand circular polarization (RHCP) or left hand circular polarization (LHCP) mode depending upon the positioning of the slots in the ground. A sequential phase (SP) feeding network based wideband 2×2 array antenna operating at 5 GHz is designed in [7] for wearable applications. The developed design consists of four aperture-coupled patch antennas which are sequentially rotated. Circular Polarization in the device is obtained by feeding the antennas with incremental 90° input phases. A metasurface-based antenna is proposed for realizing a wideband circularly polarized antenna. However, the proposed antenna has a colossal size compared to the recently proposed antennas for wearable applications. In this connection, authors in [11] have proposed a wideband CP antenna based on the SP concept for wearable applications. The prototype is compact in size, has a wider 3 dB AR beamwidth and bandwidth than the recently reported prototypes. After a thorough investigation of the designs reported in the literature, it is concluded that for biomedical applications, there is a need for an optimal antenna design that is compact, multiband, flexible, circularly polarized, minimal SAR, and also should have lower complexity.

Therefore, in this communication, we propose a circularly polarized, metasurface inspired compact antenna with dual band mode of operation for wearable biomedical applications covering Industrial, Scientific, and Medicine (ISM) band and MedRadio bands simultaneously. The usage of metasurface ensures compact size whereas single layer antenna design with optimal performance ensures that the complexity of the designed structure is minimized. The designed radiating patch consists of diagonally opposite truncated corners with 2×3 MTM unit cells engraved upon it. The 2×3 array of metastructure results in an obvious improvement in gain and circular polarization. Also, partial ground incorporated with slots is utilized for making the proposed structure operate in the desired frequency bands.

2. ANTENNA GEOMETRY

2.1. Study of Metamaterial Unit Cell

The layout of a metamaterial (MTM) unit cell designed on an RT-Duroid Rogers substrate with relative permittivity of 2.94 and dielectric loss tangent of 0.0009 is illustrated in Figure 1. The dimensions of

Table 1. Optimized dimensions of the MTM unit cell and squiggle.

Parameter	Value (mm)	Parameter	Value (mm)
L	6	J	0.6
W	5.5	k	2.5
g	1.5	z	1.5
h	2.6	S_0	2
S_C	2	S_l	6.5
S_w	2	S_i	1

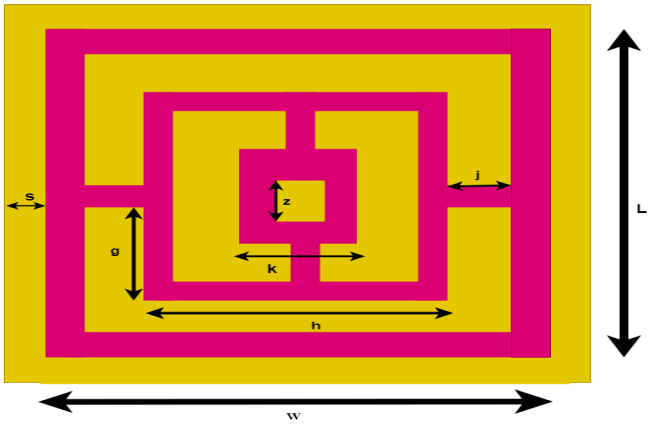

Figure 1. Layout of the proposed unit cell. Pink part depicts metallization.

the optimized MTM unit cell along with the squiggle etched out of the radiating patch are illustrated in Table 1. The design of the proposed unit cell is inspired form a conventional square split ring resonator and exhibits epsilon negative (ENG) and near-zero refractive index (NZI) in the desired operational frequency range of 2.35–2.67 GHz and 3.4–4.8 GHz. The designed structure consists of two rectangular rings with a vertical I-shaped slot in the inner rectangular patch. The outer ring is connected to the inner ring at the two opposite positions in the horizontal plane whereas the inner ring is connected to the rectangular patch at two positions in the vertical plane. The permittivity and permeability of a unit cell can be extracted in the following manner [18]:

i. A unit cell of MTM is encased in a two-port system with lattice vectors in all the three dimensions.
ii. Once the unit cell is encased, appropriate excitations and boundary conditions are assigned to the different surfaces of the three-dimensional two-port system unit element to simulate the periodic metamaterial in the electromagnetic (EM) tool.
iii. An electromagnetic plane wave is normally incident on the metamaterial as shown in Figure 2.
iv. Once S parameters of the MTM unit cell are evaluated, the permittivity, permeability, and refractive index of the design can be extracted from the below defined equations (using MATLAB script or

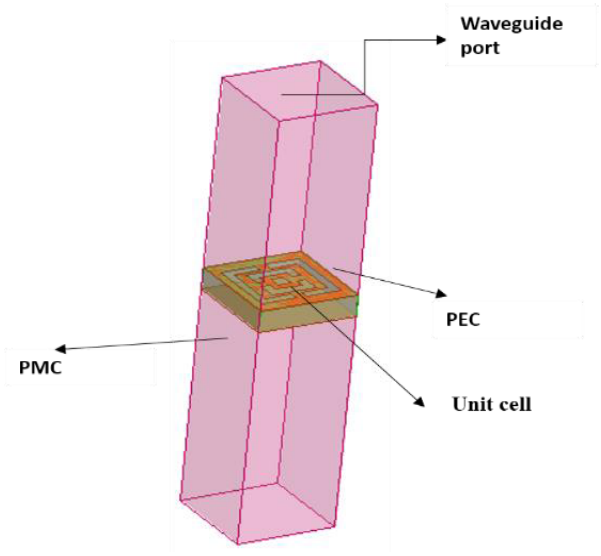

Figure 2. Simulation setup for MTM unit cell.

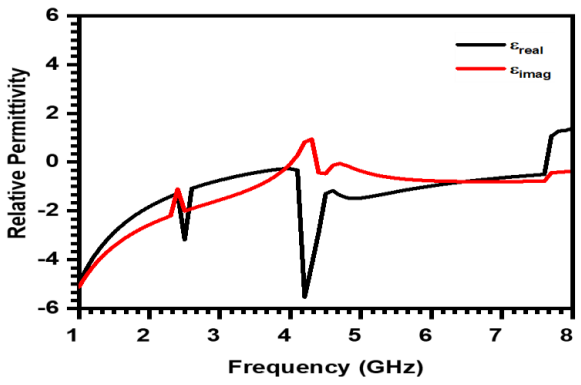

Figure 3. Permittivity plot of MTM unit cell.

HFSS calculator)

$$z = \pm\sqrt{\frac{(1+S_{11})^2 - S_{21}^2}{(1-S_{11})^2 - S_{21}^2}} \tag{1}$$

$$e^{ink_0d} = \frac{S_{21}}{1 - S_{11} \times \dfrac{z-1}{z+1}} \tag{2}$$

$$n = \frac{1}{k_0 d}\left[\left\{\left[\ln\left(e^{ink_0d}\right)\right]^{complex} + 2m\pi\right\} - i\left[\left[\ln\left(e^{ink_0d}\right)\right]^{real}\right]\right] \tag{3}$$

$$\varepsilon = \frac{n}{z}, \quad \mu = n \times z \tag{4}$$

In this work, the unit cell is designed as a Perfect Electric Conductor (PEC) on a Rogers substrate (RT Duroid 6002) with relative permittivity of 2.94, and dielectric loss tangent of 0.0012. Figure 2 illustrates the unit cell under the test whereas effective permittivity of the cell extracted is plotted in Figure 3.

2.2. Evolution of the Prospective Antenna Design

The 2×3 MTM unit cells are engraved on the radiating element of the design along with the two U-shaped loops engraved at the bottom of the patch. Partial ground with two pairs of open L-shaped slots is utilized in the design. Figure 4 provides insight about the structure of the design. The process of designing a circularly polarized antenna in this communication has been achieved in the following manner:

i. An MTM unit cell is designed with the help of an EM tool exhibiting ENG behavior in the desired frequency band.
ii. A conventional microstrip patch operating in sub-6 GHz range is designed for wearable bio-medical applications.
iii. The conventional radiating patch is loaded with an array of MTM unit cells (antenna design #1) for achieving compactness, improved radiation efficiency, and acceptable SAR on loading the antenna on human body.
iv. To achieve the circular polarization, corners of the square radiating patch are truncated (antenna design #4), and two parasitic elements are placed along the truncated portion for improving the axial ratio of the design (antenna design #5).
v. The radiating patch of the antenna is mirrored, and its effect on antenna performance is observed (antenna design #6).

3. EVALUATION OF THE ELECTROMAGNETIC (EM) RESPONSE OF THE DESIGN

Figure 4 demonstrates the layout of the antennas designed in a phased manner. In the first step, a conventional square-shaped radiating patch is designed on a Rogers 6002 substrate with the antenna resonating at 2.4 GHz and 3.85 GHz in free space. The design has a compact size of $0.264\lambda_0 \times 0.264\lambda_0 \times 0.014\lambda_0$ (33 mm × 33 mm × 1.75 mm) with λ_0 being the wavelength corresponding to the lowest resonant frequency of the design. The MTM unit cells are engraved upon the radiating patch to achieve compactness of the design ensuring that the design operates in the desired frequency band. The simulated and measured results obtained in free space are in good agreement with each other. The electromagnetic response of the design is evaluated in a phased manner in a commercially available Finite Element Method Electromagnetic tool, HFSS v 15.

The proposed antenna operates in the two frequency bands covering 2.35–2.67 GHz and 3.4–4.8 GHz as is evident from Figure 5. Furthermore, the plots clearly demonstrate how the reflection coefficient response varies with the change in the topology of the radiating element of antenna. With incorporation

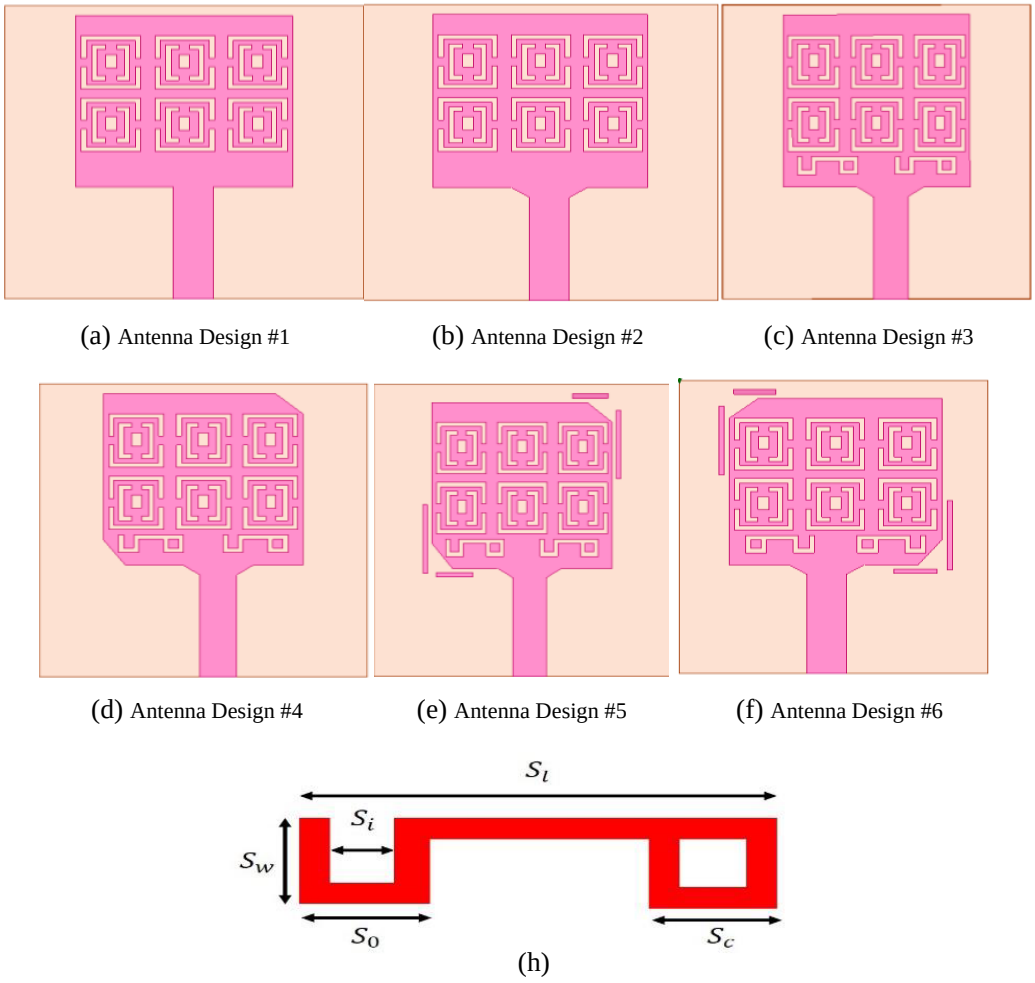

(a) Antenna Design #1 (b) Antenna Design #2 (c) Antenna Design #3

(d) Antenna Design #4 (e) Antenna Design #5 (f) Antenna Design #6

(h)

Figure 4. Evolution of the antenna design and layout of the squiggle engraved in the patch.

of different elements in radiating patch, the impedance matching becomes better in both the bands in sub-6 GHz range as illustrated in Figure 5(a). However, the antenna initially resonates at 3.8 GHz when no slots are incorporated in the partial ground, but an additional resonance creeps in the plot at 6.5 GHz when a pair of inverted smaller L-shaped slots are employed in the partial ground. The additional resonance at 2.4 GHz is incorporated when a pair of bigger L-shaped slots are engraved in the partial ground as illustrated in Figure 5(b). So, when the pair of both the slots (bigger and smaller) are engraved in the ground, a dual-band antenna with better impedance matching in both the operating bands is achieved. For achieving circular polarization, corners of the radiating patch are truncated in the next stage, and the metallic strips along the truncated corners are incorporated.

Figure 7 portrays the distribution of the surface current in the radiating patch at $\emptyset = 0°, 90°, 180°$ and 270° in Design #5 and #6. In Design #5, it is observed that at $\emptyset = 0°$ and $\emptyset = 180°$, high current density flows along the vertical direction of the radiating element in $+x$ and $-x$ direction, respectively. Similarly, it is observed that high current density flows along the horizontal direction of the patch in $-y$ and $+y$ directions for $\emptyset = 90°$ and 270°, respectively. It is concluded from these observations that the predominant currents for $\emptyset = 0°$ and 90° have equal magnitude but are opposite in phase with $\emptyset = 180°$ and 270°, respectively. Thus, the dominant portion of current flows in the clockwise direction on the basis of which it is concluded that the prospective design shows left-handed circularly polarization (LHCP) behavior in Design #5. Similarly, from Figure 7, it is observed that when the patch is mirrored, the current flows in the anticlockwise direction and hence exhibits right-handed circularly polarization (RHCP) behavior in Design #6.

Furthermore, the bandwidth over which the axial ratio (AR) is below 3 dB (approximately) is illustrated in Figure 6. It is illustrated in the figure that the AR bandwidth and impedance bandwidth overlap over a maximum portion of the two frequency bands. Furthermore, the 3 dB AR beamwidth is around 40° for the structure when it is mounted on the body. On evaluating the different performance parameters of the antenna on human phantom (by placing the antenna at a distance of 10 mm above it), it is observed that there is negligible change in the reflection coefficient of the prototype. Figure 9 illustrates the on-body plot of reflection coefficient for simulated and measured scenarios, clearly depicting that the antenna resonates at 2.45 GHz and 4.1 GHz respectively in two bands. It is observed that there is a slight change in the frequency response of the antenna in presence of the human body due to its dispersive nature. The antenna placed in the proximity of body resonates in two frequency

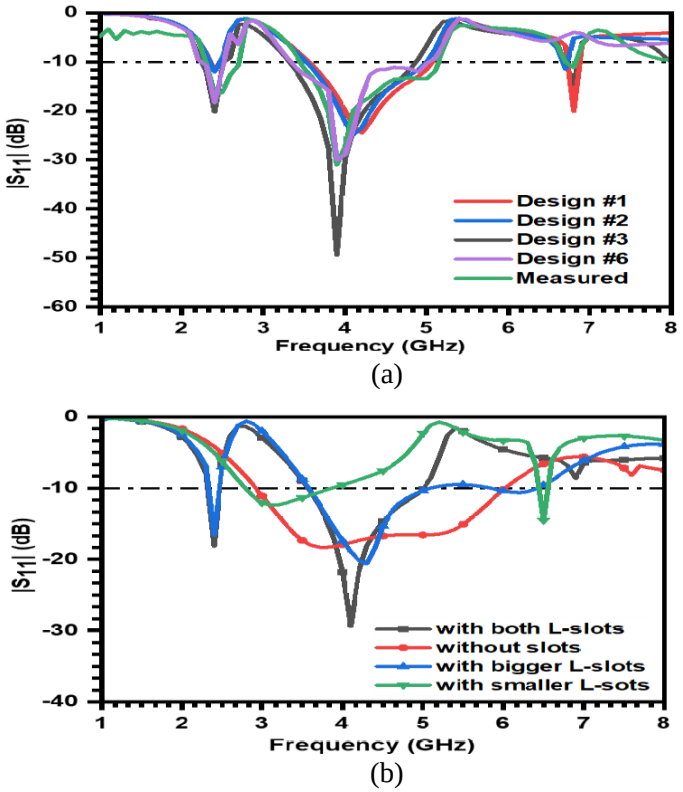

Figure 5. Return loss vs. frequency plot of the design in free space (a) change in topology of radiating patch, (b) change in topology of ground plane.

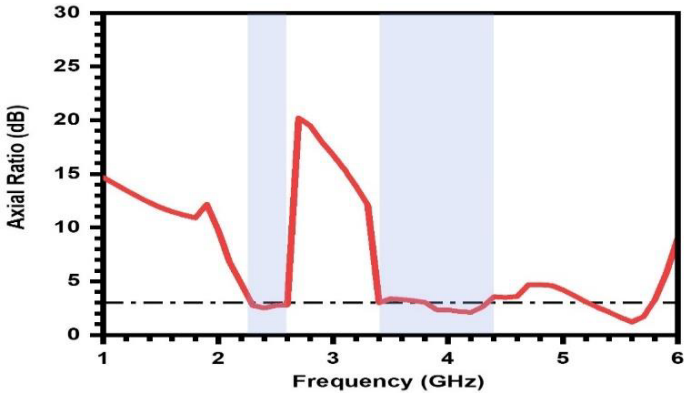

Figure 6. Axial ratio (AR) vs. frequency plot of the prototype.

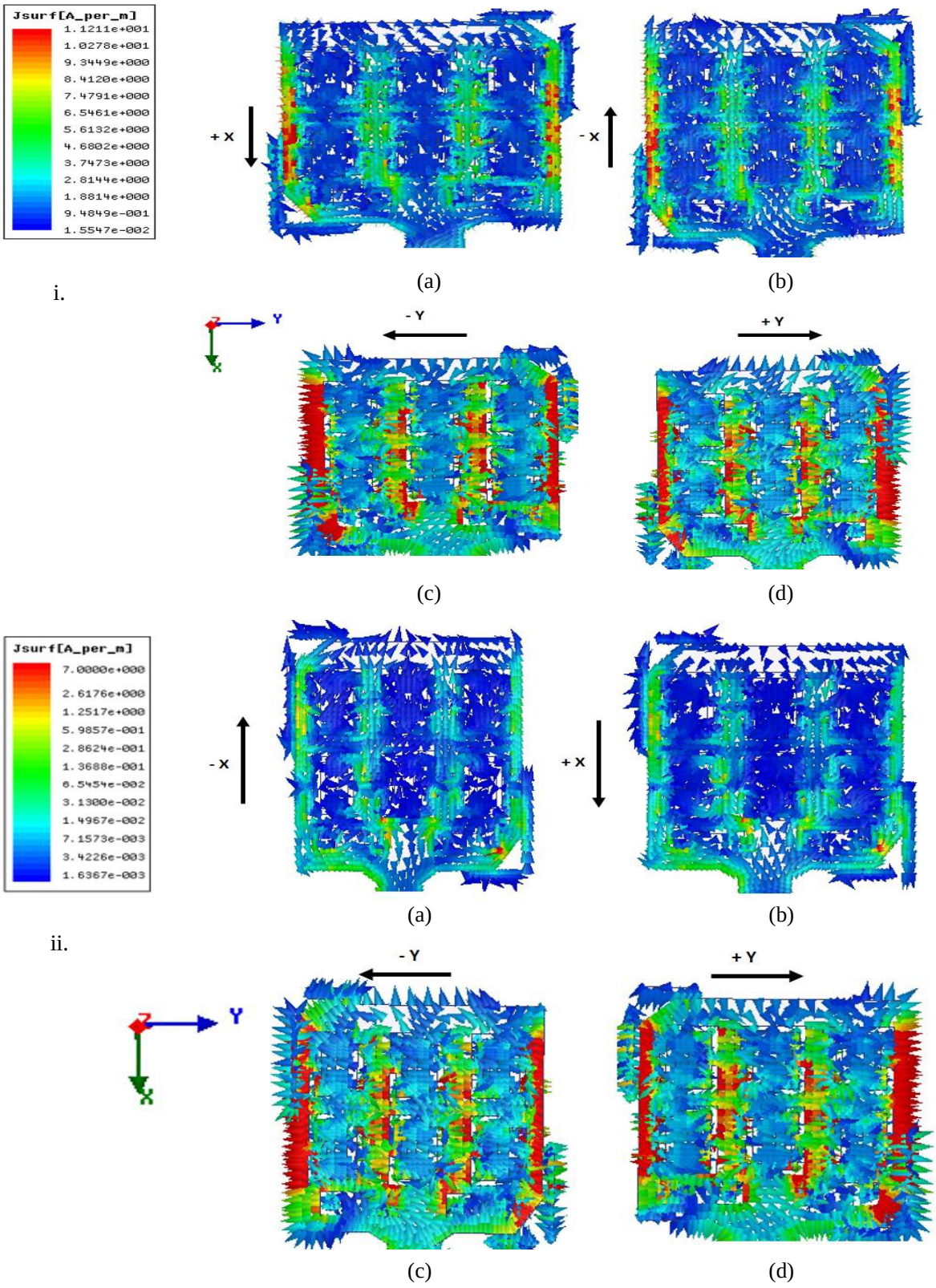

Figure 7. Surface current distribution in the proposed patch for i. Design #5, ii. Design #6. (a) $\emptyset = 0°$, (b) $\emptyset = 180°$, (c) $\emptyset = 90°$, (d) $\emptyset = 270°$.

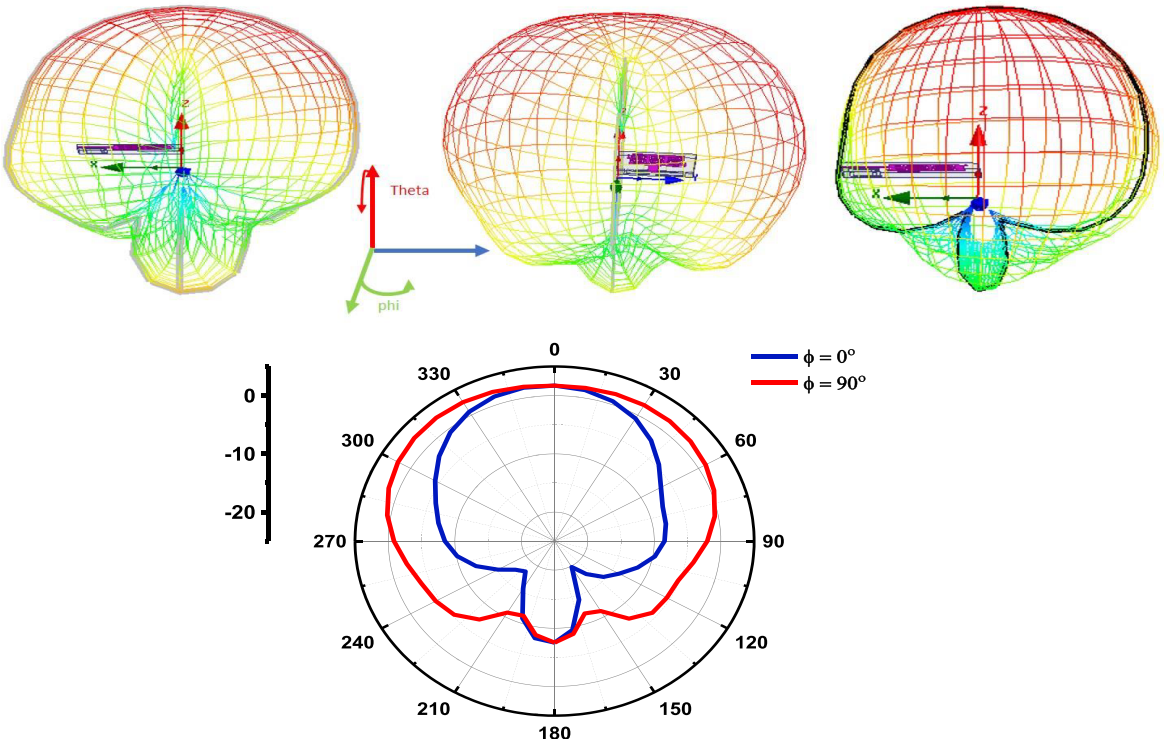

Figure 8. Radiation pattern of antenna when mounted on body.

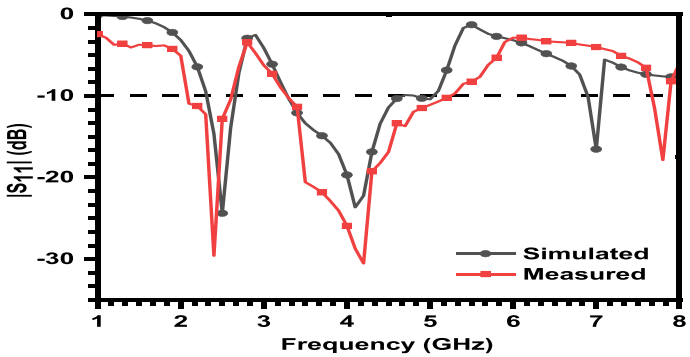

Figure 9. On-body reflection coefficient vs. frequency plot.

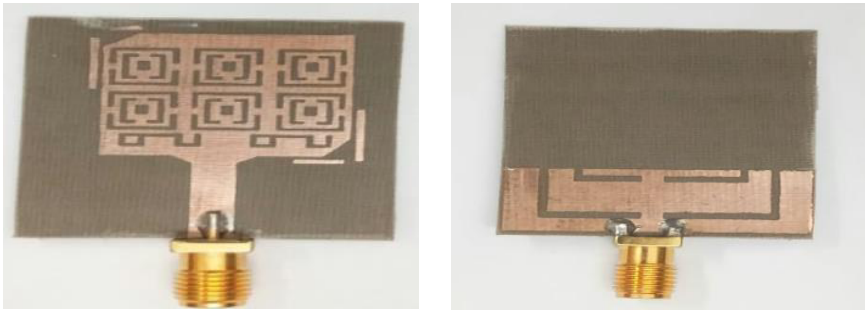

(a) (b)

Figure 10. Fabricated antenna prototype. (a) Top view. (b) Bottom view.

bands comprising 2.31–2.67 GHz and 3.28–5.04 GHz. The far field gain pattern of the design placed above 10 mm from human phantom is shown in Figure 8. The multilayered human phantom designed in this work comprises four tissue layers; skin, fat, muscle, and bone as designed in [8]. From Figure 8, it is seen that the patterns are directional with back lobe interacting with the tissue resulting in diminishing of the gain whereas the reported antenna has nearly an omnidirectional radiation pattern in free space with a peak gain of 4.3 dBi.

Figure 10 illustrates the layout of the fabricated design, whereas in Figure 11 the prototype under test in an anechoic chamber is demonstrated. On applying the input power of 10 dBm, the average Specific Absorption Rate (SAR) of the antenna over 10 g tissues is 0.0232 W/kg as depicted in Figure 12, which is well below the standard threshold values. The radiation efficiency of over 55% is observed

Figure 11. Fabricated prototype under test.

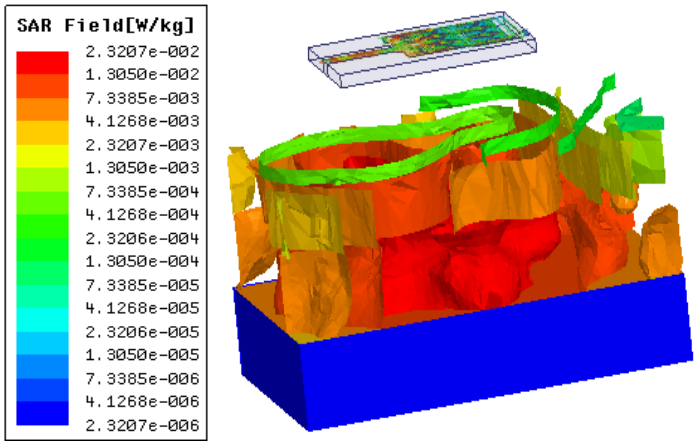

Figure 12. Specific absorption rate of the prospective antenna when mounted on multilayer human tissue.

Table 2. Parameters of SAR at 2.4 GHz [24].

Parameter	Value
Input Power for Simulation setup	10 mW
Accepted Power	9 mW
Radiated power	6 mW
Average SAR (W/kg) for 10 gram	0.023207
Relative Permittivity of skin, fat, muscle, bone (hand module)	31.29, 4.602, 52.79, 12.66
Conductivity of skin, fat, muscle, bone (hand module) S/m	8.013, 0.585, 1.705, 3.859
Loss tangent of skin, fat, muscle, bone	0.2835, 0.1938, 0.2419, 0.252

throughout the frequency range of operation. Parameters of SAR [24] for a volume of 10 g mass of multilayer tissue is discussed in Table 2.

In Table 3, state of art comparison is carried out with the recently proposed designs. It is evident that our prototype is way more compact than the other prototypes while at the same time ensuring optimal performance in all the other parameters.

Table 3. Comparative examination of the prospective design with the recently reported antennas for biomedical applications.

Ref.	f_0	Fractional Bandwidth (%)	Volume (λ_0^3)	Gain (dB)	SAR	Polarization
[13]	2.45/3/3.45	4.4/4/6.2	$0.5 \times 0.5 \times 0.06$	4.2/6.6/5	0.13/0.09	LP
[14]	2.45/6.5	4.8/3.7	$0.82 \times 0.82 \times 0.016$	5.8/6.9	0.642/0.09	LP/CP
[15]	2.45/5.8	7/52	$0.51 \times 0.51 \times 0.08$	2.2/8.6	1.04/0.29	LP/CP
[16]	2.45/5.8	NA	$0.2 \times 0.2 \times 0.02$	−0.6/4.3	2.52	LP
[12]	2.45/3.7/5.8/UWB	5.5/8.2/5.3/72.8	$0.4 \times 0.4 \times 0.12$	1/6.6/5.05/6.5	1.5/0.83/0.36/0.06	LP/CP
[17]	2.4	4.5	$0.44 \times 0.44 \times 0.045$	5.2	0.294	CP
[11]	5.48	43	$0.73 \times 0.73 \times 0.07$	7.5	NA	CP
Prop.	2.45/4.1	14.4/43	$0.264 \times 0.264 \times 0.014$	1.88–3.03	0.023	CP

4. LINK BUDGET ANALYSIS

In order to examine the ability of our wearable antenna to communicate, the antenna at the receiving end is placed away from the body in free space at an optimum distance. To know about this optimum distance, the communication link budget analysis is carried out using Friis power transmission formula [9, 10].

$$P_r\,(\text{dBm}) = G_r\,(\text{dB}) + G_t\,(\text{dB}) + P_t\,(\text{dBm}) - PL(d) \tag{5}$$

where PL is the distance dependent path loss in multipath propagation environment and can be calculated using Equation (2).

$$PL_{\text{dB}}(d) = 10n \log\left(\frac{d}{d_0}\right) + 20 \log\left(\frac{4\pi d_0}{\lambda}\right) + \chi_\sigma \tag{6}$$

where n is the path loss exponent with its value depending on the type of communication; G_r and G_t represent the gains of the receiver and transmitting antenna, respectively. Furthermore, the χ_σ symbolizes the shadowing factor for normal distribution with standard deviation σ. The value of n in

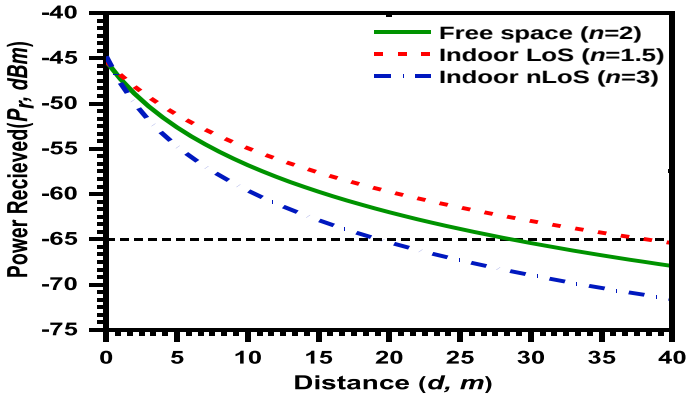

Figure 13. Received power as the function of distance.

this study has been accounted for three scenarios; $n = 1$ for free space propagation, $n = 1.5$ for indoor Line of Sight propagation(hall, lobby etc.), and $n = 3$ for indoor non-Line of sight (nLoS) propagation. For link budget analysis, a dipole antenna (Circularly Polarized) with a gain of 2 dBi is adopted for the role of the receiver antenna in the designed antenna system. The transmitting power is kept at 10 dBm (10 mW), keeping in consideration that the design is going to be used for biomedical applications. The reference distance (d_0) is kept as 1 m, frequency of operation as 2.45 GHz, and thereof, the variation of received power (dBm) with the distance is plotted in Figure 13. It is observed that for the indoor Line of Sight (LoS) propagation scenario, the power received by the antenna exceeds −65 dBm at a distance of 40 m for the transmitting power of 10 dBm. In case of indoor nLoS (densely packed rooms etc.), the power received is more than −65 dBm at a distance of 20 m for the same transmitting power. Assuming that the minimum receiver sensitivity (in terms of power level) is −65 dBm, a reliable communication link is ensured within 40 m for LoS and 20 m for then LoS environment.

5. CONCLUSION

In this article, the authors have addressed the major issues of wearable antennas meant for different biomedical applications. Metamaterial (MTM) inspired dual-band circularly polarized antenna covering MedRadio and Industrial, Scientific, and Medicine (ISM) band is proposed, fabricated, and validated in different scenarios. The prospective antenna operates in the two frequency bands of 2.31 GHz–2.67 GHz and 3.28 GHz–5.04 GHz ensuring wide 3 dB AR bandwidth/beamwidth, comparatively lower SAR, substantial gain, and reasonable radiation efficiency with compact size in comparison to the recently proposed antennas. Communicating ability of the antenna within the indoor ranges (up to 40 m) has also been evaluated in the article.

ACKNOWLEDGMENT

University Grants Commission, Ministry of Education has supported this work under grant No. 3725/(NET-JULY2018).

REFERENCES

1. Zada, M., I. A. Shah, and H. Yoo, "Metamaterial-loaded compact high-gain dual-band circularly polarized implantable antenna system for multiple biomedical applications," *IEEE Transactions on Antennas and Propagation*, Vol. 68, No. 2, 1140–1144, Feb. 2020, doi: 10.1109/TAP.2019.2938573.
2. Ramli, K. N., R. A. Abd-Alhameed, C. H. See, P. S. Excell, and J. M. Noras, "Hybrid computational scheme for antenna-human body interaction," *Progress In Electromagnetics Research*, Vol. 133, 117–136, 2012.
3. Kibret, B., A. K. Teshome, and D. Lai, "Human body as antenna and its effect on human body communications," *Progress In Electromagnetics Research*, Vol. 148, 193–207, 2014.
4. Malik, N. A., P. Sant, T. Ajmal, and M. Ur-Rehman, "Implantable antennas for bio-medical applications," *IEEE Journal of Electromagnetics RF and Microwaves in Medicine and Biology*, Vol. 5, No. 1, 84–96, 2021.
5. Chaouche, Y. B., M. Nedil, I. B. Mabrouk, and O. M. Ramahi, "A wearable circularly polarized antenna backed by AMC reflector for WBAN communications," *IEEE Access*, Vol. 10, 12838–12852, 2022, doi: 10.1109/ACCESS.2022.3146386.
6. Kaim, V., B. K. Kanaujia, S. Kumar, H. C. Choi, K. W. Kim, and K. Rambabu, "Ultra-miniature circularly polarized CPW-fed implantable antenna design and its validation for biotelemetry applications," *Scientific Reports*, Vol. 10, No. 1, 1–16, 2020.
7. Chen, Y., X. Liu, Y. Fan, and H. Yang, "Wearable wideband circularly polarized array antenna for off-body applications," *IEEE Antennas and Wireless Propagation Letters*, Vol. 21, No. 5, 1051–1055, 2022.

8. Khan, U. R., J. A. Sheikh, A. Junaid, R. Amin, S. Ashraf, and S. Ahmed, "Design of a compact hybrid Moore's fractal inspired wearable antenna for IoT enabled bio-telemetry in diagnostic health monitoring system," *IEEE Access*, Vol. 10, 116129–116140, 2022, doi: 10.1109/ACCESS.2022.3219442.
9. Yang, H. C., X. Y. Liu, Y. Fan, and M. M. Tentzeris, "Flexible circularly polarized antenna with axial ratio bandwidth enhancement for off-body communications," *IET Microw. Antennas Propag.*, Vol. 15, 754–767, 2021.
10. Iqbal, A., A. Smida, A. J. Alazemi, M. I. Waly, N. K. Mallat, and S. Kim, "Wideband circularly polarized MIMO antenna for high data wearable biotelemetric devices," *IEEE Access*, Vol. 8, 17935–17944, 2020, doi: 10.1109/ACCESS.2020.2967397.
11. Chen, Y., X. Liu, Y. Fan, and H. Yang, "Wearable wideband circularly polarized array antenna for off-body applications," *IEEE Antennas and Wireless Propagation Letters*, Vol. 21, No. 5, 1051–1055, May 2022, doi: 10.1109/LAWP.2022.3157367.
12. Le, T. T., Y.-D. Kim, and T. Y. Yun, "Wearable pattern-diversity dual-polarized button antenna for versatile on-/off-body communications," *IEEE Access*, Vol. 10, 98700–98711, 2022, doi: 10.1109/ACCESS.2022.3206799.
13. Le, T. T., Y.-D. Kim, and T. Y. Yun, "A triple-band dual-open-ring high gain high-efficiency antenna for wearable applications," *IEEE Access*, Vol. 9, 118435–118442, 2021.
14. Zhou, L., S. Fang, and X. Jia, "Dual-band and dual-polarised circular patch textile antenna for on-/off-body WBAN applications," *IET Microw. Antennas Propag.*, Vol. 14, No. 7, 643–648, Jun. 2020.
15. Yin, X., S. J. Chen, and C. Fumeaux, "Wearable dual-band dual polarization button antenna for WBAN applications," *IEEE Antennas Wireless Propag. Lett.*, Vol. 19, No. 12, 2240–2244, Dec. 2020.
16. Zhang, X. Y., H. Wong, T. Mo, and Y. F. Cao, "Dual-band dual-mode button antenna for on-body and off-body communication," *IEEE Transactions on Biomedical Circuits and Systems*, Vol. 11, No. 4, 933–941, Aug. 2017.
17. Jiang, Z. H., M. D. Gregory, and D. H. Werner, "Design and experimental investigation of a compact circularly polarized integrated filtering antenna for wearable biotelemetric devices," *IEEE Transactions on Biomedical Circuits and Systems*, Vol. 10, No. 2, 328–338, Apr. 2016, doi: 10.1109/TBCAS.2015.2438551.
18. Numan, A. B. and M. S. Sharawi, "Extraction of material parameters for metamaterials using a full-wave simulator [Education Column]," *IEEE Antennas and Propagation Magazine*, Vol. 55, No. 5, 202–211, Oct. 2013, doi: 10.1109/MAP.2013.6735515.
19. Mishra, N. and R. K. Chaudhary, "A miniaturized ZOR antenna with enhanced bandwidth for WiMAX applications," *Microwave and Optical Technology Letters*, Vol. 58, 2016.
20. Mishra, N. and R. K. Chaudhary, "A compact wideband short-ended metamaterial antenna for wireless applications," *Progress In Electromagnetics Research Letters*, Vol. 66, 93–98, 2017.
21. Mishra, N. and R. K. Chaudhary, "A compact CPW fed CRR loaded four element metamaterial array antenna for wireless application," *Progress In Electromagnetics Research*, Vol. 159, 15–26, 2017.
22. Mishra, N. and R. Chaudhary, "A miniaturized directive high gain metamaterial antenna using ELC ground for WiMAX application," *International Journal of Electronics Letters*, Vol. 7, 2018, doi: 10.1080/21681724.2018.1426112.
23. Kumar, S. and R. Kumari, "Composite right/left-handed ultra-wideband metamaterial antenna with improved gain," *Microwave and Optical Technology Letters*, Vol. 63, 2020, doi: 10.1002/mop.32552.
24. Pimienta Del Valle, D. and R. Lagar-Pérez, "Design of a dual-band PIFA for handset devices and it SAR evaluation," *Ingeniería, Investigación y Tecnología*, Vol. 17, 169–178, 2016, doi: 10.1016/j.riit.2016.06.002.